# A novel approach to determining the three-dimensional location of microscopic objects with applications to 3D particle tracking

Sripad Ram[a,b], Jerry Chao[a,c], Prashant Prabhat[a,c], E. Sally Ward[a] and Raimund J. Ober[a,c]

[a] Center for Immunology, University of Texas Southwestern Medical Center, Dallas, TX, USA;
[b] Joint Biomedical Engineering Graduate Program, University of Texas at Arlington/University of Texas Southwestern Medical Center, Dallas, TX, USA;
[c] Department of Electrical Engineering, University of Texas at Dallas, Richardson, TX, USA.

## ABSTRACT

Recent technological advances have rendered widefield fluorescence microscopy as an invaluable tool to image fast dynamics of trafficking events in two dimensions (i.e., in the plane of focus). Three-dimensional trafficking events are studied by sequentially imaging different planes within the specimen by moving the plane of focus with a focusing device. However, these devices are typically slow and hence when the cell is being imaged at one focal plane, important events could be missed at other focal planes. To overcome this limitation, we recently developed a novel imaging technique called multifocal plane microscopy that enables the simultaneous imaging of multiple focal planes within the sample. Here, by using tools of information theory, we present a quantitative evaluation of this technique in the context of 3D particle tracking. We calculate the Fisher information matrix for the problem of determining the 3D location of an object that is imaged on a multifocal plane setup. In this way, we derive a lower bound on the accuracy with which the object can be localized in 3D. We illustrate our results by considering the object of interest to be a single molecule. It is well known that a conventional widefield microscope has poor depth discrimination capability and therefore there exists significant uncertainty in determining the axial location of the object, especially when it is close to the plane of focus. Our results predict that the multifocal plane microscope setup offers improved accuracy in determining the axial location of objects than a conventional widefield microscope.

**Keywords:** multifocal plane microscopy, single molecule microscopy, 3D localization accuracy, Fisher information matrix, Cramer-Rao inequality, 3D single molecule tracking

## 1. INTRODUCTION

Particle tracking experiments in live biological samples provide invaluable insights into the dynamics of biological processes. Of practical importance in tracking experiments is to know the accuracy with which the location of the particle/object of interest can be determined. One of the shortcomings of conventional widefield optical microscopes is their poor depth discrimination capability.[1] Due to this, there exists significant uncertainty in determining the axial location of objects such as single molecules, especially when they are close to the plane of focus. Previously we showed that the limit of the 3D localization accuracy of a single molecule can significantly vary depending upon the defocus level.[2] For instance, for small defocus values ($\leq$ 200 nm), it was predicted that the $x_0/y_0$ coordinate of the single molecule can be determined with relatively high accuracy whereas the $z_0$ coordinate can be determined with poor accuracy. On the other hand, for large defocus values (200 - 700 nm), it was predicted that the $x_0/y_0$ coordinate of the single molecule can be determined with poor accuracy whereas the $z_0$ coordinate can be determined with high accuracy. Due to this mismatch in the limit of the localization accuracy between the $x_0/y_0$ coordinate and the $z_0$ coordinate, it is difficult to determine all three coordinates with the same level of accuracy.

To overcome this problem, we propose to use the multifocal plane imaging technique that was previously developed by our group.[3,4] Here we simultaneously image two distinct focal planes within the specimen. One focal plane corresponds to the standard focal plane that is imaged in a conventional widefield microscope, while the other focal plane corresponds to a plane that is shifted away from the standard focal plane. If the object of interest (single molecules) is imaged in the above setup, then the image of the shifted focal plane provides additional information regarding the object location. By making use of this additional data, we expect to obtain higher accuracy in determining the location of the object. An alternative to the multifocal plane imaging technique is to use a focusing device, which *sequentially* moves the objective lens to acquire images of the different focal planes. A drawback with this approach is that focusing devices are typically slow and moreover, suffer from the lack of synchrony between their movement and the movement of the object in the specimen. Thus when the specimen is being imaged at one focal plane important events can be missed in the other planes. With the multifocal plane imaging approach these problems are avoided, since there is no movement of the objective lens and more importantly the specimen is simultaneously imaged at multiple planes.

## 2. MULTIFOCAL PLANE MICROSCOPY
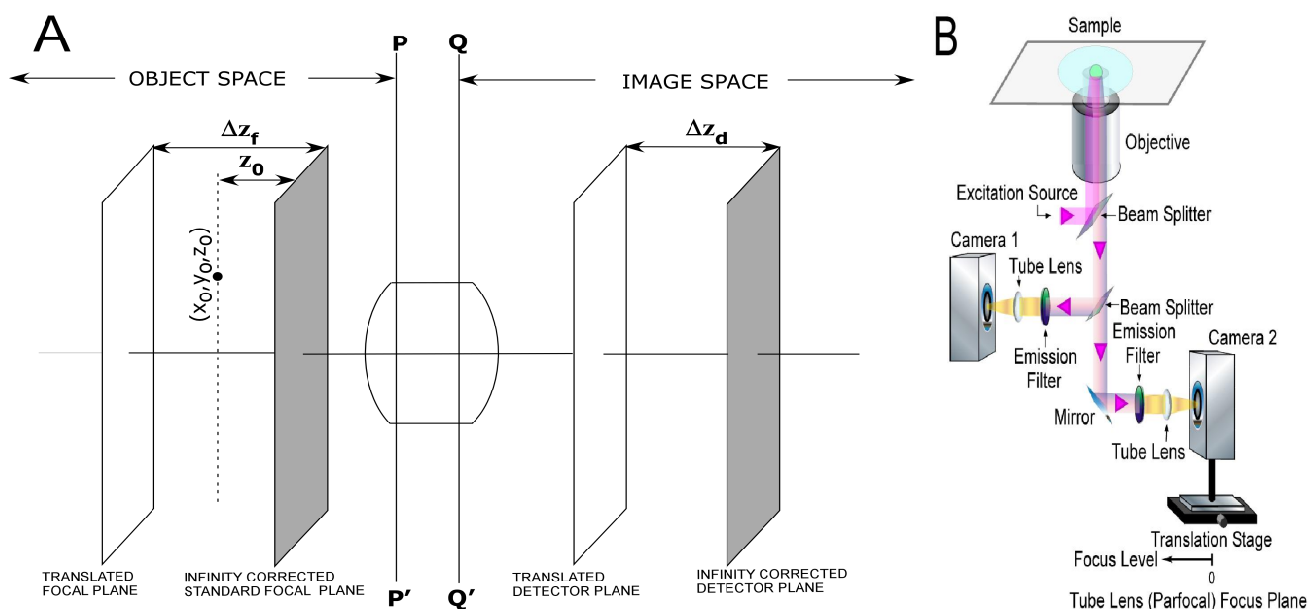


**Figure 1.** Panel A shows the principle of multifocal plane imaging. The schematic shows how a detector position different from the typical infinity corrected position results in the imaging of a focal plane that is further from the objective lens than the focal plane corresponding to the standard configuration. Panel B shows the layout for a multifocal plane imaging setup with two imaging detectors.[3]

The basic principle of multifocal plane imaging technique is illustrated in Fig. 1A. A detailed discussion of this technique can be found elsewhere[3,4] and here we provide a brief description. In the standard fluorescence microscope, the detector is located at the infinity corrected detector plane and captures the image of a thin section of the specimen that coincides with the infinity corrected standard focal plane. If, however, the detector is moved towards the microscope optics (i.e., to the translated detector plane), then the detector captures the focal plane that is further from the infinity corrected standard focal plane. Fig. 1B shows a simple realization of this principle where two distinct focal planes within the sample are simultaneously imaged. Here, the collected fluorescence light from the objective lens is split by a beam splitter into two light paths. In each of those two light paths emission filters are followed by a tube lens that focuses the image onto the detector. In one of the light paths, the imaging detector is placed at the focal length of the tube lens and this corresponds to the standard/design detector position in an optical microscope. In the other light path, the imaging detector is

mounted on a translation stage. By changing the position of this detector relative to the tube lens, a focal plane within the specimen that is distinct from the standard infinity-corrected focal plane (i.e., design focal plane) is imaged.

## 3. RESULTS

### 3.1. General approach

The task of determining the 3D location of an object from multifocal plane imaging data is a parameter estimation problem, where the location coordinates $(x_0, y_0, z_0)$ of the single molecule are estimated from the acquired data. To predict the achievable accuracy in the multifocal plane imaging setup, we calculate the Fisher information matrix for this estimation problem. The Fisher information matrix provides a quantitative measure of the total information contained in the acquired data about the parameter that we wish to estimate. According to the Cramer-Rao inequality,[5] the (co)variance (matrix) of any unbiased estimator $\hat{\theta}$ of $\theta$ is always greater or equal to the inverse Fisher information matrix, i.e., $\text{Cov}(\hat{\theta}) \geq \mathbf{I}^{-1}(\theta)$. In parameter estimation problems, the accuracy of the estimates is specified in terms of its standard deviation. From the above inequality, it follows that the square root of the (corresponding leading diagonal entry of the) inverse Fisher information matrix provides a lower bound to the accuracy of the estimates of $\theta$. In the present context, if $\theta$ denotes the 3D location of the object then the square root of the (leading diagonal entries of the) inverse Fisher information matrix provides a *limit* to the accuracy with which the 3D location coordinates can be determined in the multifocal plane setup.

### 3.2. Calculation of the Fisher information matrix

An important property of the Fisher information matrix is that it is independent of the estimation procedure used to estimate the parameter $\theta$ and only depends on the statistical nature of the acquired data. The acquired data is modeled as a spatio-temporal random process, which is referred to as the image detection process $\mathcal{G}$.[6] The temporal part is an inhomogeneous Poisson process that models the time points of the detected photons and the spatial part is a sequence of independent random variables that models the location coordinates at which the photons hit the detector. In the multifocal plane imaging setup, the data acquired from each focal plane can be described by an independent image detection process. Hence the Fisher information matrix for the 3D location estimation problem in a two plane imaging setup is given by

$$\mathbf{I}_{tot}(\theta) := \mathbf{I}_{plane1}(\theta) + \mathbf{I}_{plane2}(\theta), \tag{1}$$

where $\theta = (x_0, y_0, z_0)$ denotes the 3D location of the object, $\mathbf{I}_{plane1}(\theta)$ and $\mathbf{I}_{plane2}(\theta)$ denote the Fisher information matrices of the image detection processes that describe the acquired data from the two focal planes. For the two plane imaging setup shown in Fig. 1, one of the focal planes corresponds to the design plane and the other focal plane corresponds to the shifted plane. Without loss of generality we set plane 1 to correspond to the standard infinity-corrected (design) focal plane. The Fisher information matrix for data acquired from focal plane 1 is given by[2, 6]

$$\mathbf{I}_{plane1}(\theta) := \text{diag}\left[ \int_{t_0}^{t} \int_{\mathbb{R}^2} \frac{\Lambda(\tau)}{q_{z_0}(x,y)} \left( \frac{\partial q_{z_0}(x,y)}{\partial x} \right)^2 dxdyd\tau \quad \int_{t_0}^{t} \int_{\mathbb{R}^2} \frac{\Lambda(\tau)}{q_{z_0}(x,y)} \left( \frac{\partial q_{z_0}(x,y)}{\partial y} \right)^2 dxdyd\tau \right.$$

$$\left. \int_{t_0}^{t} \int_{\mathbb{R}^2} \frac{\Lambda(\tau)}{q_{z_0}(x,y)} \left( \frac{\partial q_{z_0}(x,y)}{\partial z_0} \right)^2 dxdyd\tau \right], \quad \theta \in \Theta, \tag{2}$$

where $\Lambda$ and $q_{z_0}$ denote the photon detection rate and the image function of the object, respectively. An image function $q_{z_0}$ describes the image of an object at unit magnification that is located at $(0, 0, z_0)$ in the object space.[6] The expression of $\mathbf{I}_{plane2}(\theta)$ will be analogous to that of eq. 2, but with $z_0$ replaced by $z_0 - \Delta z_f$, where $z_0$ denotes the axial coordinate of the single molecule with respect to the design focal plane and $\Delta z_f$ denotes the axial distance between the design focal plane and the shifted focal plane in the object space (see Fig. 1A). Note that the above expression of the Fisher information matrix is applicable to a wide variety of imaging conditions including polarized excitation and/or detection.

### 3.3. 3D image of single molecule

For the present discussion we consider the object of interest to be a single molecule. From eq. 2 we see that to calculate the Fisher information matrix for the two focal planes, we require an analytical expression for the image function of the single molecule $q_{z_0}$. For this, we use the Gibson and Lanni model[7] of the 3D point spread function to describe the 3D image of a single molecule, which in terms of the image function is given by[2]

$$q_{z_0}(x,y) = \frac{1}{C_{z_0}} \left| \int_0^1 J_0 \left( ka\rho \frac{\sqrt{x^2+y^2}}{z_d} \right) \exp(jW_{z_0}(\rho))\rho d\rho \right|^2, \quad (x,y) \in \mathbb{R}^2, \quad z_0 \in \mathbb{R}, \tag{3}$$

where $(x,y) \in \mathbb{R}^2$ denotes an arbitrary point on the detector plane, $z_d$ denotes the axial distance of the detector from the back focal plane of the microscope lens system, $C_{z_0}$ is the normalization constant such that $\int_{\mathbb{R}^2} q_{z_0}(x,y)dxdy = 1$, $k = 2\pi/\lambda$, $\lambda$ denotes the wavelength of the detected photons, $a$ denotes the radius of the limiting aperture of the microscope projected onto the back focal plane of the lens system, $J_0$ denotes the zeroth order Bessel function of the first kind and $W_{z_0}(\rho)$ denotes the phase aberration term. We note that eq. 3 provides a general expression for several 3D point spread function models,[7] which describe the image of a point-source/single-molecule and are based on scalar diffraction theory.

### 3.4. 2D fundamental limit and the in focus scenario

A special case of the 3D image of the single molecule concerns the in focus scenario where the defocus distance $z_0$ is equal to zero. Substituting for $z_0 = 0$ in eq. 3, the image function $q_{z_0}$ reduces to the classical Airy profile, which is given by $q(x,y) := J_1^2(\alpha\sqrt{x^2+y^2})/(\pi(x^2+y^2))$, $(x,y) \in \mathbb{R}^2$, where $\alpha := 2\pi n_a/\lambda$ and $n_a$ denotes the numerical aperture of the objective lens. Substituting this in eq. 2, we obtain the fundamental limit to the 2D localization accuracy of the single molecule that is given by (see Ref. 8 for details)

$$\delta_{x_0}^{2d} = \delta_{y_0}^{2d} = \frac{\lambda}{2\pi n_a \sqrt{\Lambda_0(t-t_0)}}, \qquad \textbf{(2D fundamental limit)} \tag{4}$$

where $[t_0, t]$ denotes the acquisition time interval and $\Lambda_0$ denotes the photon detection rate of the single molecule.

### 3.5. Multifocal plane 3D fundamental limit

Substituting $q_{z_0}$ given in eq. 3 in $\mathbf{I}_{plane1}(\theta)$ (and $\mathbf{I}_{plane2}(\theta)$) we obtain the expression for $\mathbf{I}_{tot}(\theta)$. Then by using the Cramer-Rao inequality, we define the multifocal plane fundamental limit to the 3D localization accuracy of a single molecule as the square root of the leading diagonal entries of $\mathbf{I}_{tot}^{-1}(\theta)$ (henceforth referred to as the multifocal plane 3D fundamental limit). We denote this result as *fundamental*, since the data model that underlies the derivation of this result does not take into account deteriorating experimental factors. Hence this formula provides the best-case scenario for a given imaging condition.

To calculate the 3D fundamental limit, we require an explicit analytical expression for the phase aberration term $W_{z_0}$ and here, we set $W_{z_0}$ to be

$$W_{z_0}(\rho) := \frac{\pi(n_a)^2 z_0}{n_{oil}\lambda}\rho^2, \quad \rho \in (0,1), \quad z_0 \in \mathbb{R}, \tag{5}$$

where $n_a$ denotes the numerical aperture of the objective lens, and $n_{oil}$ denotes the refractive index of the immersion oil. The above expression for $W_{z_0}$ corresponds to the classical 'Born and Wolf' 3D point spread function model.[9] When analyzing data from single molecule experiments, the intensity function $\Lambda$ is typically assumed to be a constant. Hence in the present context, the intensity function is given by $\Lambda(\tau) := \Lambda_0$, $\tau \geq t_0$, where $\Lambda_0$ denotes the photon detection rate of the single molecule.

Figure 2A shows the multifocal 3D fundamental limit of $x_0/y_0$ as a function of defocus for a two plane imaging setup. The figure also shows the 3D fundamental limit of $x_0/y_0$, which pertains to the conventional widefield microscope, and the 2D fundamental limit of $x_0/y_0$, which pertains to the in focus scenario and is given by eq. 4. Here we set the single molecule location to be $(0,0,z_0)$, i.e., the single molecule is located on the
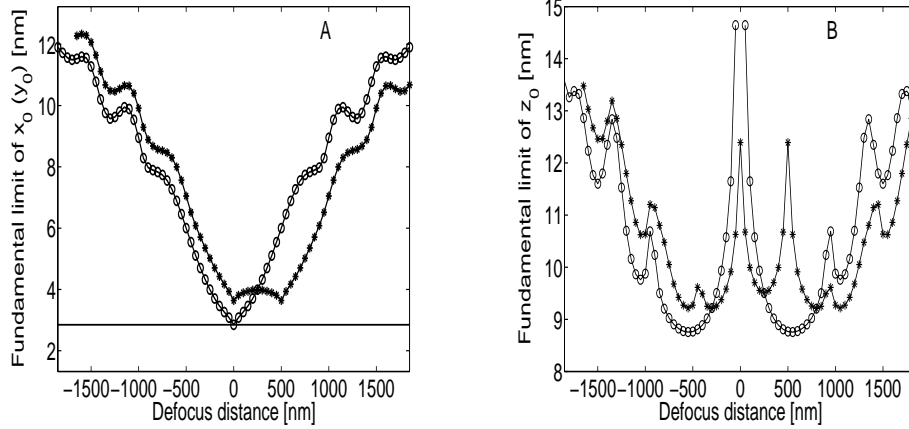
**Figure 2.** Behavior of the 3D fundamental limit as a function of defocus distance ($z_0$). Panel A shows the fundamental limit of the localization accuracy of the $x_0$ ($y_0$) coordinate of a single-molecule/point-source as a function of defocus distance and Panel B shows that same for the $z_0$ coordinate. In both panels, ($\circ$) denotes the 3D fundamental limit for the conventional microscope setup, ($*$) denotes the multifocal 3D fundamental limit for a two plane imaging setup with a plane spacing of $\Delta z_f = 500$ nm, and (——) denotes the 2D fundamental limit of $x_0$ for the conventional microscope setup. For the calculation of the 2D and 3D fundamental limit for the conventional microscope setup, the single molecule location is set to be (0,0,$z_0$), the photon detection rate is set to be $\Lambda_0 = 5000$ photons/s, the acquisition time is set to be $t = 0.1$ s (with $t_0 = 0$), the numerical aperture is set to be $NA = 1.3$, the magnification is set to be $M = 100$. For the multifocal plane 3D fundamental limit, the single molecule location is set to be (0,0,$z_0 - \Delta z_f$) where $\Delta z_f$ denotes the spacing between plane 1 and plane 2, and the photon detection rate is set to half the value used for the conventional microscope setup calculations, since in the two plane imaging setup the emission light is split into two paths. The numerical values of all other parameters are identical to those used for the conventional microscope setup calculations.

optical axis (z-axis) of the objective lens in the object space, where $z_0$ denotes the defocus distance from the plane of focus (plane 1) of the objective lens. Previously, we had shown that the 3D fundamental limit of $x_0$ in a conventional microscope setup deteriorates with increasing defocus distances and is symmetric about $z_0 = 0$.[2] In contrast, we see that the 3D multifocal plane fundamental limit exhibits a different behavior. Here, the multifocal plane 3D fundamental limit of $x_0$ is asymmetric about $z_0 = 0$ and remains more or less constant for a range of defocus distances. In particular, for a given focal plane spacing $\Delta z_f$, the range of defocus distances for which the multifocal plane 3D fundamental limit remains constant falls within the interval $[0 \ \Delta z_f]$. Outside this distance range, the multifocal plane 3D fundamental limit deteriorates. Note that for negative defocus distances, the 3D fundamental limit for the multifocal plane setup is consistently larger than that for the conventional microscope setup. However, in the case of positive defocus distances, the 3D fundamental limit for the multifocal plane setup is consistently smaller than that for the conventional microscope setup for a defocus distance greater than $\Delta z_f/2$. It should be pointed out that in computing the multifocal plane 3D fundamental limit, the Fisher information matrix for each focal plane was computed with the photon detection rate set to half the value that was used in the calculation of the 3D fundamental limit of a regular optical microscope. This is done to take into account the splitting of the emitted light from the single molecule into two light paths in the multifocal plane imaging setup.

Figure 2B shows the multifocal 3D fundamental limit of $z_0$ as a function of defocus for a two plane imaging setup and for a conventional microscope setup. From the figure we see that the 3D fundamental limit for the multifocal plane imaging setup is consistently smaller than that for the conventional microscope setup for defocus distances in the range of $[-\Delta z_f/2, \Delta z_f/2]$. Most importantly, the multifocal plane 3D fundamental limit of $z_0$ has a finite value when the defocus distance is zero (i.e., $z_0 = 0$). This is in contrast to the result for the conventional microscope setup, where the 3D fundamental limit of $z_0$ becomes infinitely large when $z_0 = 0$. Note that here also the multifocal plane 3D fundamental limit of $z_0$ is asymmetric about $z_0 = 0$.

## 3.6. Effects of pixelation and noise

We next investigate how experimental factors deteriorate the multifocal plane 3D fundamental limit. In particular, we consider the pixelation of the detector and the presence of extraneous noise sources, i.e., additive Poisson and additive Gaussian noise sources, in the acquired data. The general expression of the Fisher information matrix for a pixelated detector in the presence of extraneous noise sources is given by[6]

$$\mathbf{I}(\theta) := \sum_{k=1}^{N_p} \left( \frac{\partial \mu_\theta(k,t)}{\partial \theta} \right)^T \frac{\partial \mu_\theta(k,t)}{\partial \theta} \times \left( \int_{\mathbb{R}} \frac{\left( \sum_{l=1}^{\infty} \frac{[\nu_\theta(k,t)]^{l-1} e^{-\nu_\theta(k,t)}}{(l-1)!} \cdot \frac{1}{\sqrt{2\pi}\sigma_{w,k}} e^{-\frac{1}{2}\left( \frac{z-l-\eta_k}{\sigma_{w,k}} \right)^2} \right)^2}{p_{\theta,k}(z)} dz - 1 \right), \quad (6)$$

where $\theta \in \Theta$, $\nu_\theta(k,t) := \mu_\theta(k,t) + \beta(k,t)$, $k = 1, \ldots, N_p$, $\theta \in \Theta$,

$$p_{\theta,k}(z) := \frac{1}{\sqrt{2\pi}\sigma_{w,k}} \sum_{l=0}^{\infty} \frac{[\nu_\theta(k,t)]^l e^{-\nu_\theta(k,t)}}{l!} e^{-\frac{1}{2}\left( \frac{z-l-\eta_k}{\sigma_{w,k}} \right)^2}, \quad \theta \in \Theta, \quad z \in \mathbb{R},$$

$\mu_\theta(k,t)$ $(\beta(k,t))$ denotes the mean photon count from the single molecule (background component) detected at the $k^{th}$ pixel, and $\eta_k$ and $\sigma_{w,k}$ denote the mean and the standard deviation of the readout noise component at the $k^{th}$ pixel, respectively.

In deriving the above results, we made no specific assumptions on the size, shape or orientation of the pixels. Moreover, we also assume that the parameters for the noise sources are distinct at each pixel. Hence our results provide a generic framework that is applicable to a wide variety of detectors. Using these general results, we then evaluate the deterioration in the multifocal plane 3D fundamental limit for detectors with square pixels.
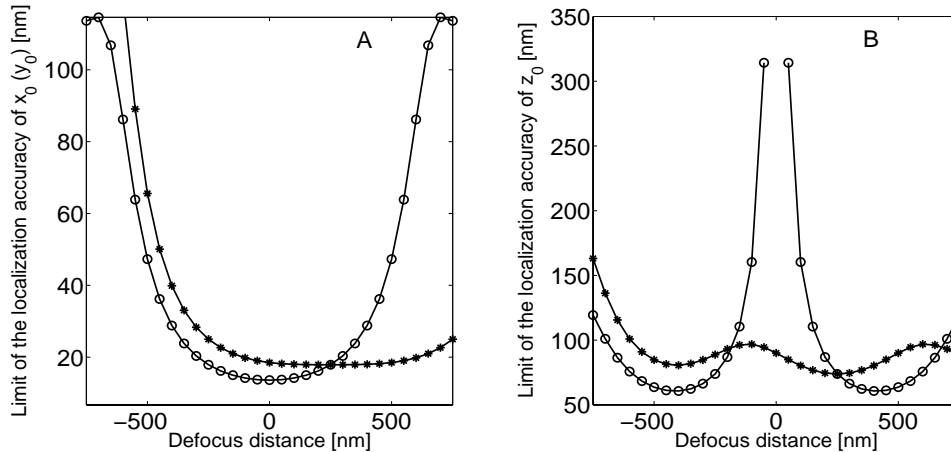


**Figure 3.** Behavior of the 3D limit of the localization accuracy as a function of defocus distance for a pixelated detector in the presence of noise sources. Panel A shows the 3D limit of the localization accuracy of the $x_0$ $(y_0)$ coordinate of a single-molecule/point-source as a function of defocus distance and Panel B shows the same for the $z_0$ coordinate. In both panels, ($\circ$) denotes the limit of the 3D localization accuracy for the conventional microscope setup and ($*$) denotes the same for the two plane imaging setup with a plane spacing of $\Delta z_f = 500$ nm. For all the plots, the pixel array size is set to $5 \times 5$, the pixel size is set to $13\mu m \times 13\mu m$, the magnification is set to 100, the exposure time is set to 0.1 s, the mean of the additive Poisson noise component is set to 25 photons/s, and the mean and standard deviation of the Gaussian noise component are set to be $\eta_k = 0$ and $\sigma_{w,k} = 8$ $e^-$ rms, respectively, the noise statistics is assumed to be the same for all the pixels and the X-Y location coordinates of the single molecule coincides with the center of the pixel array. The numerical values of all other parameters are identical to those used in Figure 2.

Figure. 3 shows the multifocal plane 3D limit of the localization accuracy of $x_0/y_0$ and $z_0$ as a function of defocus distance for a pixelated detector in the presence of extraneous noise sources. The figure also shows the 3D limit of the localization accuracy that pertains to the conventional widefield microscope setup. For all the calculations, the (x,y) coordinates of the single molecule is set to be the center of the pixel array. From the figure we see that the multifocal plane 3D limit of the localization accuracy exhibits a behavior analogous to that of the multifocal plane 3D fundamental limit shown in Figure 2. Note that in the case of the pixelated detector, the multifocal plane limit of the localization accuracy for $x_0/y_0$ coordinate is more or less constant for defocus distances in the range of 0 to 500 nm. This is in stark contrast to the 3D limit of the localization accuracy for the conventional microscope setup, in which limit of the localization accuracy of $x_0/y_0$ varies with varying defocus distances. In the case of the $z_0$ coordinate, the difference is more pronounced in the sense that there is very high uncertainty in determining the $z_0$ coordinate of a single molecule with a conventional optical microscope setup. However, this uncertainty is significantly reduced in the case of the multifocal imaging setup. An immediate implication of this result is that with a multifocal plane imaging microscope the axial ($z_0$) location of a single molecule can be determined with relatively high accuracy when compared to a conventional optical microscope setup, especially when the single molecule is close to the plane of focus.

The accuracy with which the 3D position of a single molecule can be localized has significant influence on the nature of the studies that can be carried out. Previously, it has been shown that due to the poor depth discrimination capability of conventional optical microscopes, all three coordinates of the single molecule cannot be determined with the same level of accuracy especially when the single molecule is close to the plane of focus. This implies that a conventional optical microscope setup is not well suited for tracking single molecules in 3D. The multifocal plane imaging methodology presented here overcomes this limitation and provides a novel technique for tracking single molecules in three dimensions. The calculation pertaining to the limit of the 3D localization accuracy based on the Cramer-Rao lower bound provides experimenters with a novel tool to determine apriori the best possible accuracy with which the 3D location of a single molecule can be determined. In this way, an experimenter can evaluate the feasibility of carrying out 3D tracking experiments with single molecules.

## REFERENCES

1. S. Inoue and K. R. Spring, *Video Microscopy: The fundamentals*, Plenum Press, 2nd ed., 1997.
2. S. Ram, E. S. Ward, and R. J. Ober, "How accurately can a single molecule be localized in three dimensions using a fluorescence microscope?," *Proceedings of the SPIE* **5699**, pp. 426–435, 2005.
3. P. Prabhat, S. Ram, E. S. Ward, and R. J. Ober, "Simultaneous imaging of different focal planes in fluorescence microscopy for the study of cellular dynamics in three dimensions," *IEEE Transactions on Nanobioscience* **3**(4), pp. 237–242, 2004.
4. P. Prabhat, S. Ram, E. S. Ward, and R. J. Ober, "Simultaneous imaging of several focal planes in fluorescence microscopy for the study of cellular dynamics in 3D," *Proceedings of the SPIE* **6090**, pp. 115–121, 2006.
5. C. R. Rao, *Linear statistical inference and its applications.*, Wiley, New York, USA., 1965.
6. S. Ram, E. S. Ward, and R. J. Ober, "A stochastic analysis of performance limits for optical microscopes," *Multidimensional Systems and Signal Processing* **17**, pp. 27–58, 2006.
7. S. F. F. Gibson, *Modelling the 3D imaging properties of the fluorescence light microscope.* PhD thesis, Carnegie-Mellon University, 1990.
8. R. J. Ober, S. Ram, and E. S. Ward, "Localization accuracy in single molecule microscopy," *Biophysical Journal* **86**, pp. 1185–1200, 2004.
9. M. Born and E. Wolf, *Principles of Optics*, Cambridge University Press, Cambridge, UK, 1999.